Ruthenium(II)-Diphosphine Complexes Containing Acylthiourea Ligands are Effective Against Lung and Breast Cancer

Gregory F. Grawe[a], Katia M. Oliveira[b*], Celisnolia M. Leite[a], Tamires D. de Oliveira[a], João Honorato[a], Antonio G. Ferreira[a], Eduardo E. Castellano[c], Marcia R. Cominetti[d], Rodrigo S. Correa[b], Alzir A. Batista[a,e]*

[a]*Departamento de Química, Universidade Federal de São Carlos – UFSCar, CP 676, CEP 13561-901, São Carlos, SP, Brazil*

[b]*Departamento de Química, ICEB, Universidade Federal de Ouro Preto (UFOP), CEP 35400-000, Ouro Preto – MG, Brazil*

[c]*Instituto de Física de São Carlos, Universidade de São Paulo – USP, CP 369, CEP 13560-970 São Carlos, SP, Brazil;*

[d]*Departamento de Gerontologia, Universidade Federal de São Carlos (UFSCar), CP 676, CEP 13565-905, São Carlos – SP, Brazil*

[e]*Instituto de Química, Universidade Federal de Goiás – UFG, CEP 74690-900, Goiânia, GO, Brazil.*

* Corresponding authors: e-mail: kmoliveiraq@gmail.com (K. M. Oliveira) and daab@ufscar.br (Alzir A. Batista). Tel.: +55 16 33518285; Fax: +55 16 33518350.

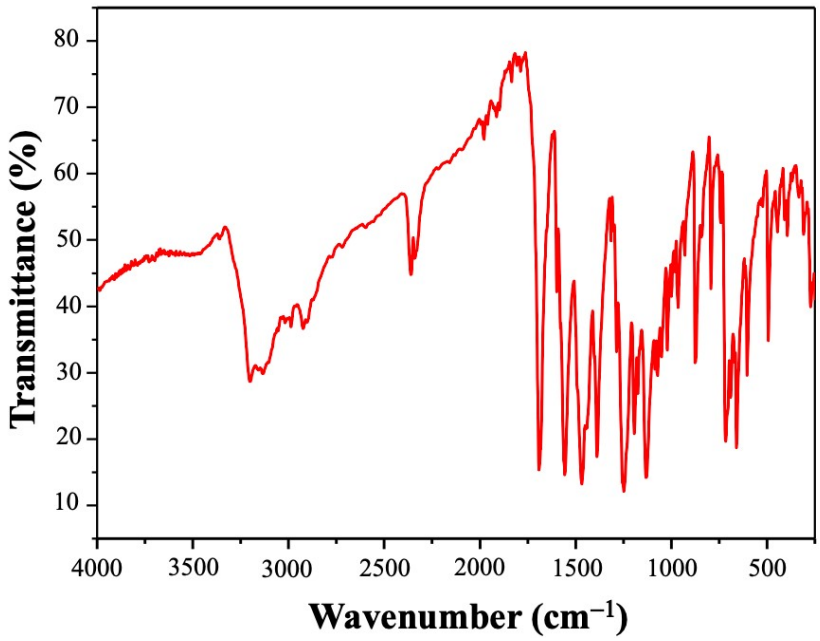

Figure S1. Infrared spectrum of the free *N,N*-dimethyl-*N'*-(benzoyl)thiourea in KBr pellets.

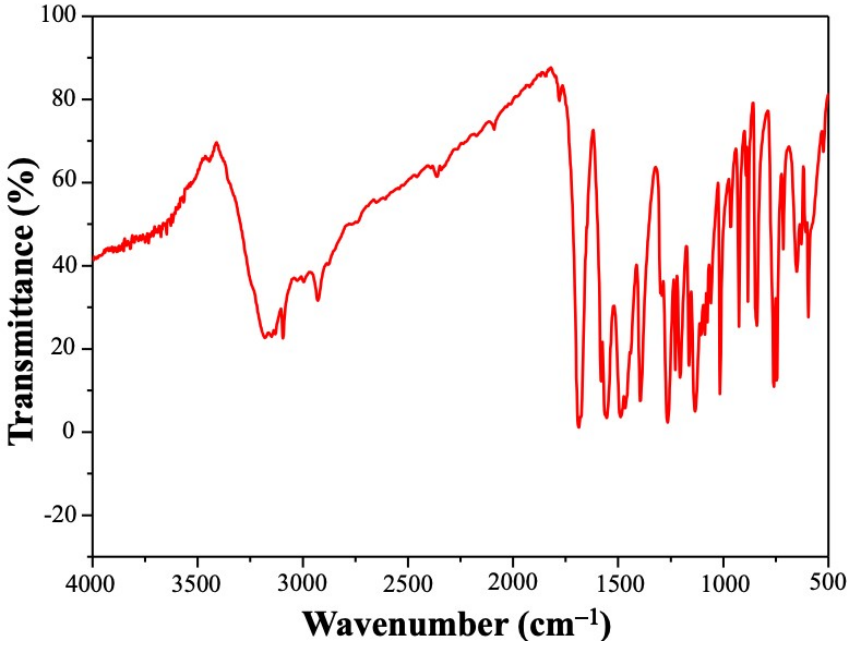

Figure S2. Infrared spectrum of the free *N,N*-dimethyl-*N'*-(furoyl)thiourea in KBr pellets.

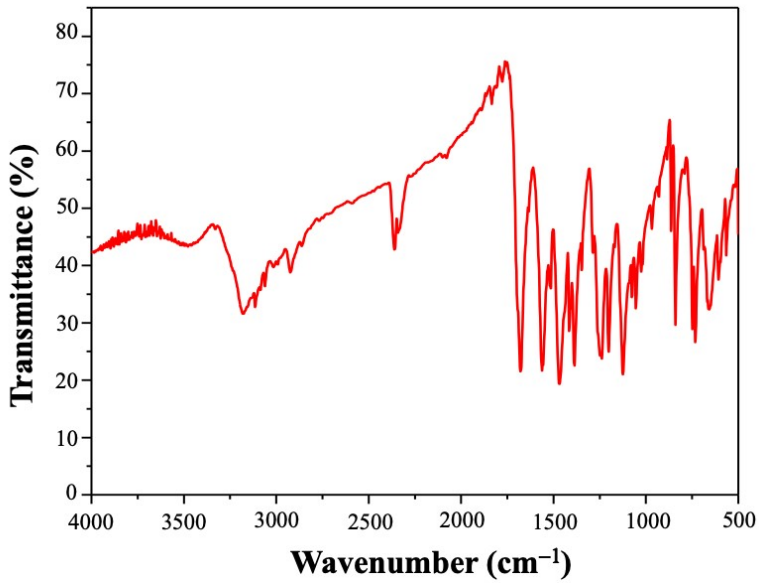

Figure S3. Infrared spectrum of the free *N,N*-dimethyl-*N'*-(thiophenyl)thiourea in KBr pellets.

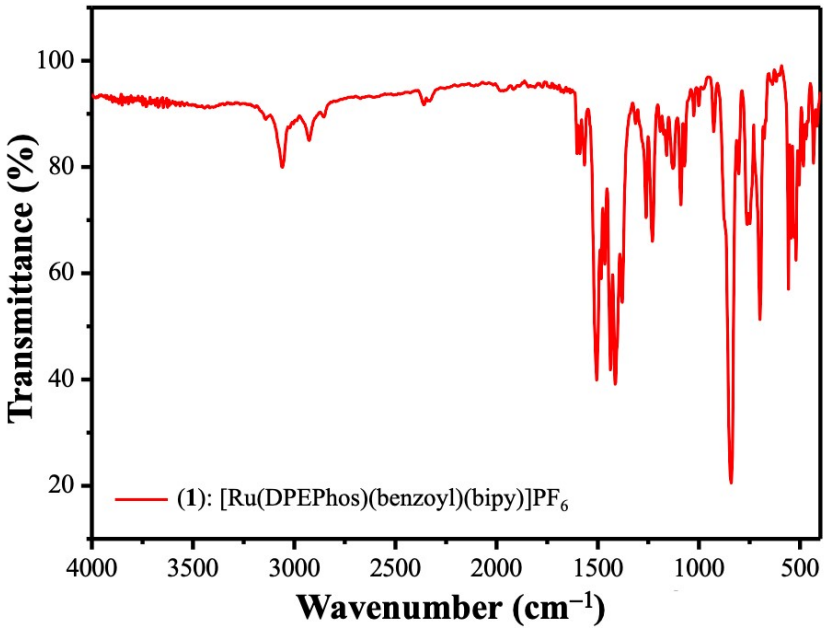

Figure S4. Infrared spectrum of the complex (**1**) in KBr pellets.

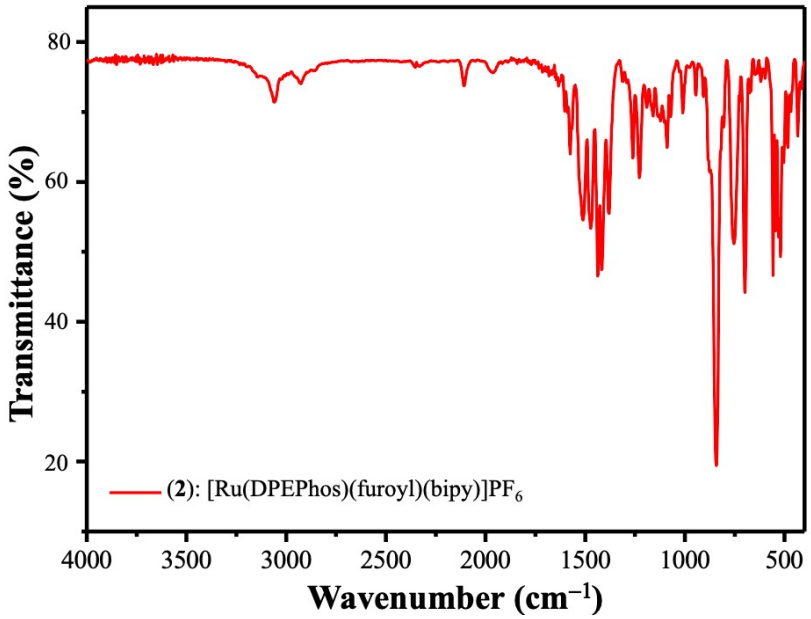

Figure S5. Infrared spectrum of the complex (**2**) in KBr pellets.

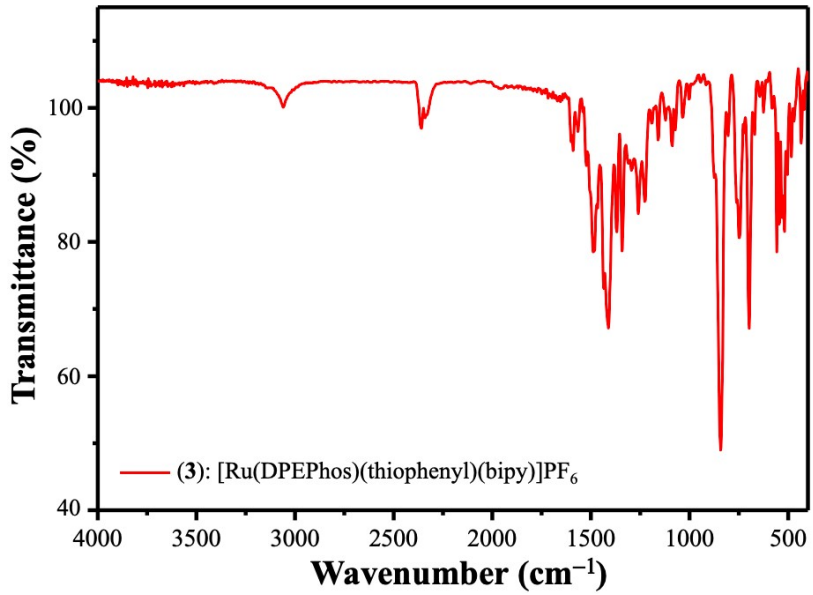

Figure S6. Infrared spectrum of the complex (**3**) in KBr pellets.

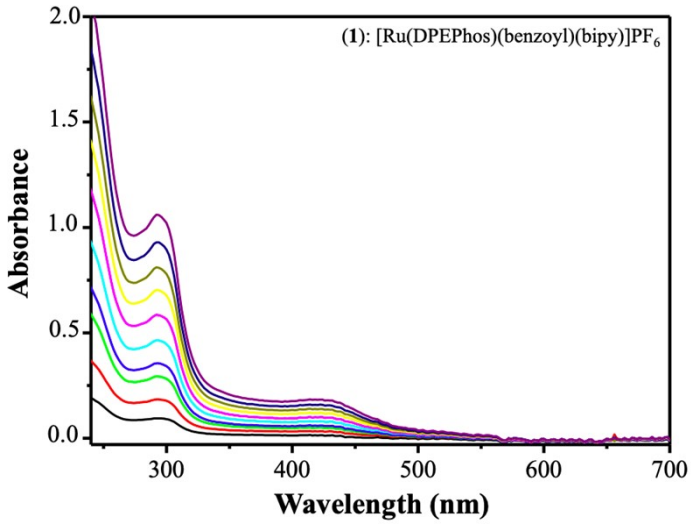

Figure S7. UV-vis spectra of the complex (**1**) in CH_2Cl_2.

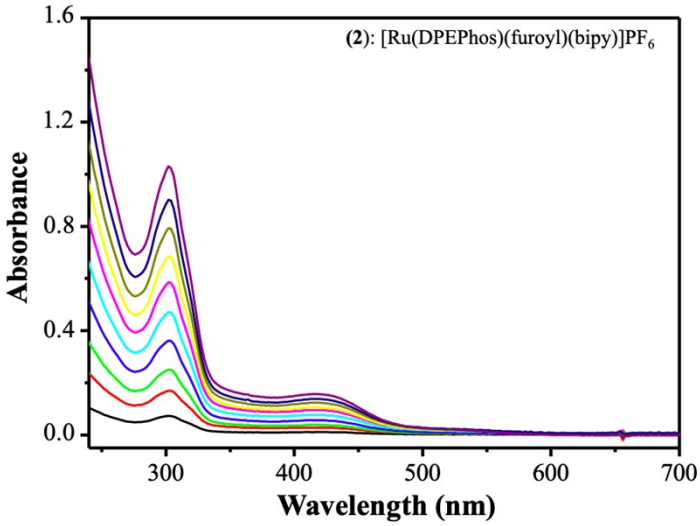

Figure S8. UV-vis spectra of the complex (**2**) in CH_2Cl_2.

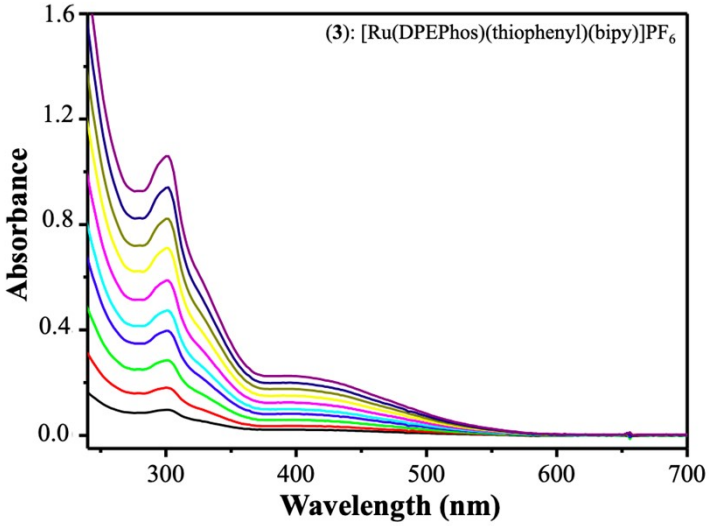

Figure S9. UV-vis spectra of the complex (**3**) in CH_2Cl_2.

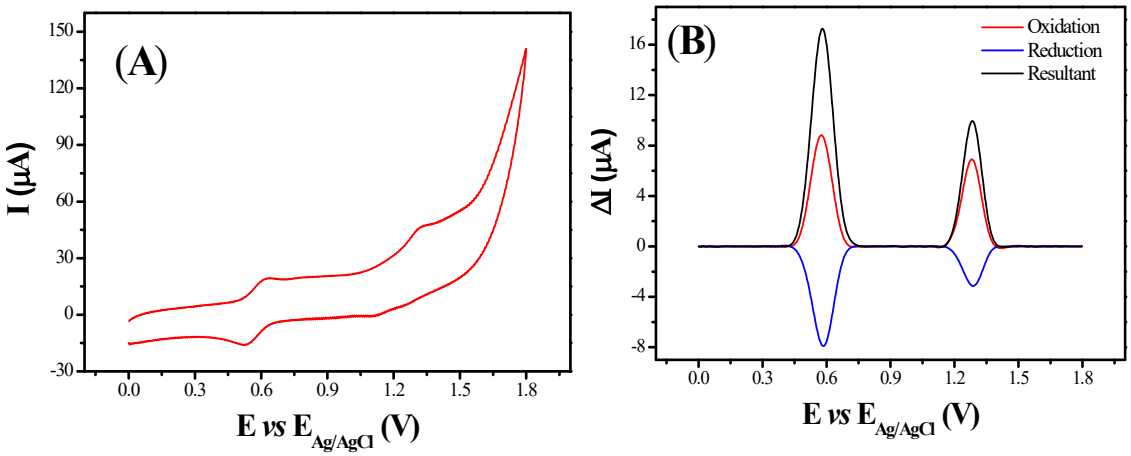

Figure S10. (**A**) Cyclic voltammogram and (**B**) square wave voltammogram of *cis*-[$RuCl_2$(DPEPhos)(bipy)], 1.0 × 10^{-3} mol L^{-1} in CH_2Cl_2 (TBAP 0.1 mol L^{-1}). V= 50 mV s^{-1}; *f* = 50 Hz; ΔE = 50 mV; E_{step} = 2.0 mV.

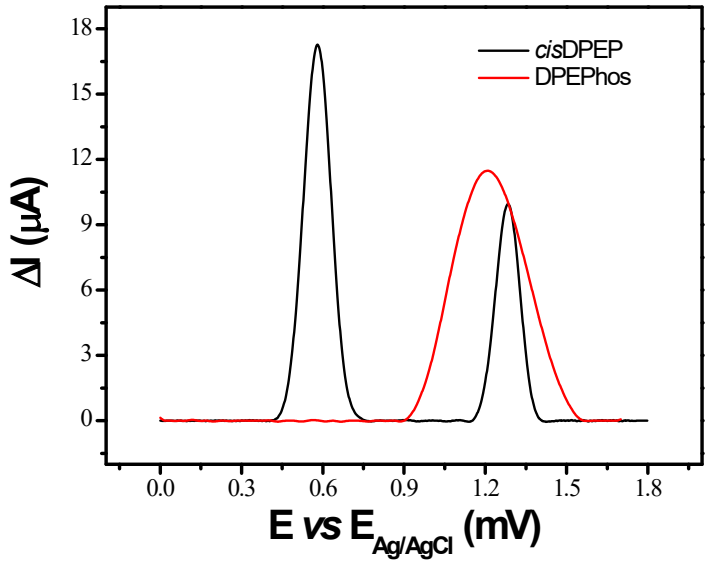

Figure S11. Square wave voltammogram of (—) *cis*-[$RuCl_2$(DPEPhos)(bipy)] and (—) DPEPhos free, both at 1.0 × 10^{-3} mol L^{-1}, in CH_2Cl_2 (TBAP 0.1 mol L^{-1}). *f* = 50 Hz; ΔE = 50 mV; E_{step} = 2.0 mV.

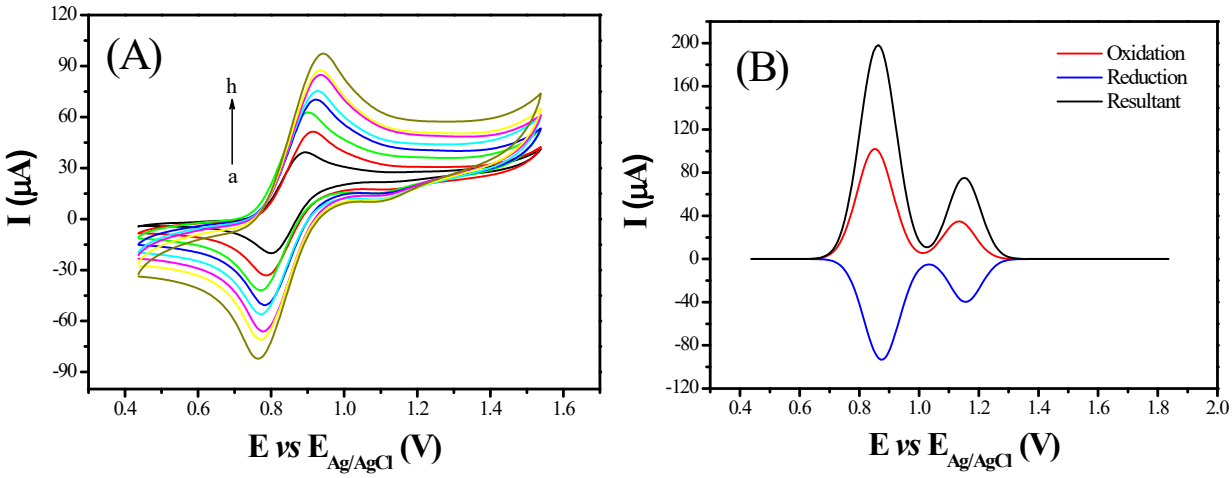

Figure S12. (**A**) Cyclic voltammogram (V = 20 – 200 mV s^{-1}) and (**B**) square wave voltammogram of complex (**2**), 1.0 × 10^{-3} mol L^{-1}, in CH_2Cl_2 (TBAP 0.1 mol L^{-1}).

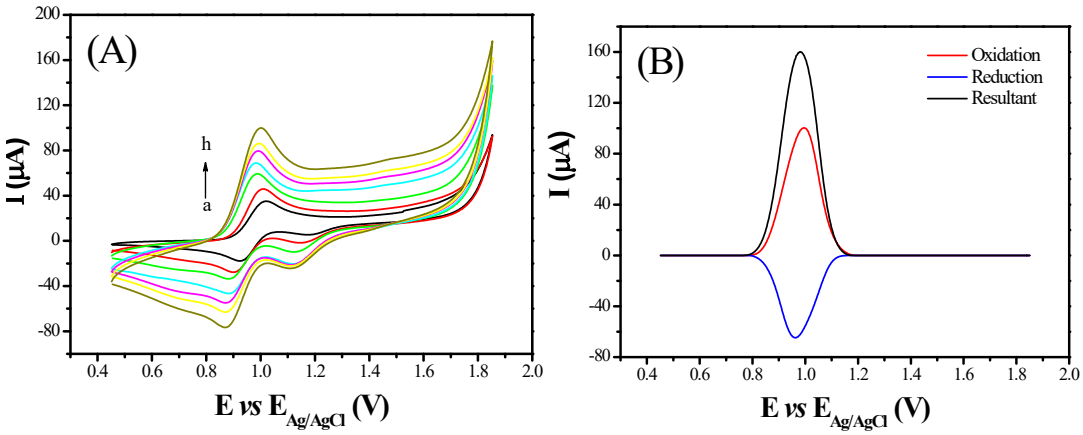

Figure S13. (**A**) Cyclic voltammogram (V = 20 - 200 mV s^{-1}) and (**B**) square wave voltammogram of complex (**3**), 1.0 × 10^{-3} mol L^{-1}, in CH_2Cl_2 (TBAP 0.1 mol L^{-1}).

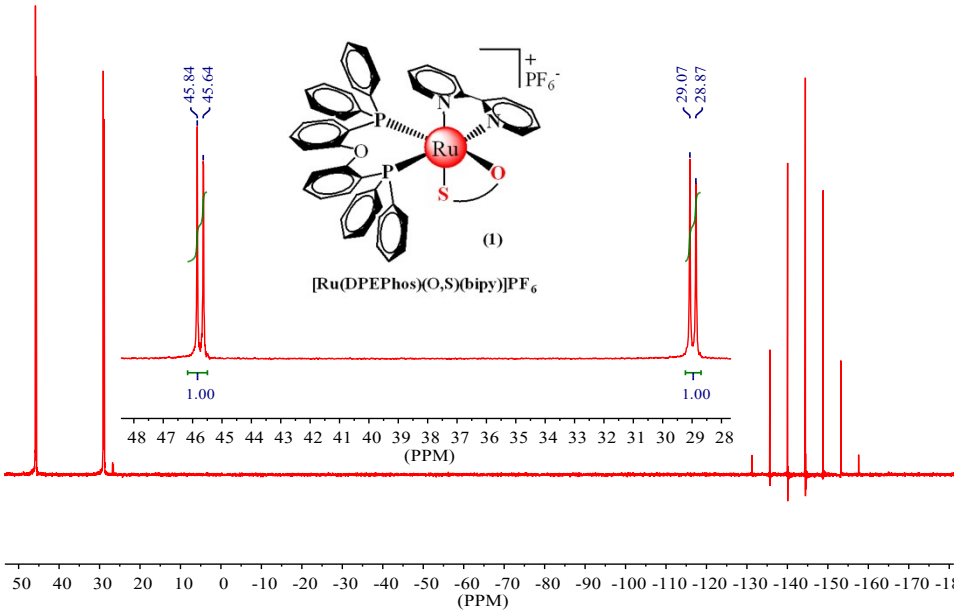

Figure S14. $^{31}P\{^1H\}$ NMR spectrum of complex (**1**) in CD_2Cl_2.

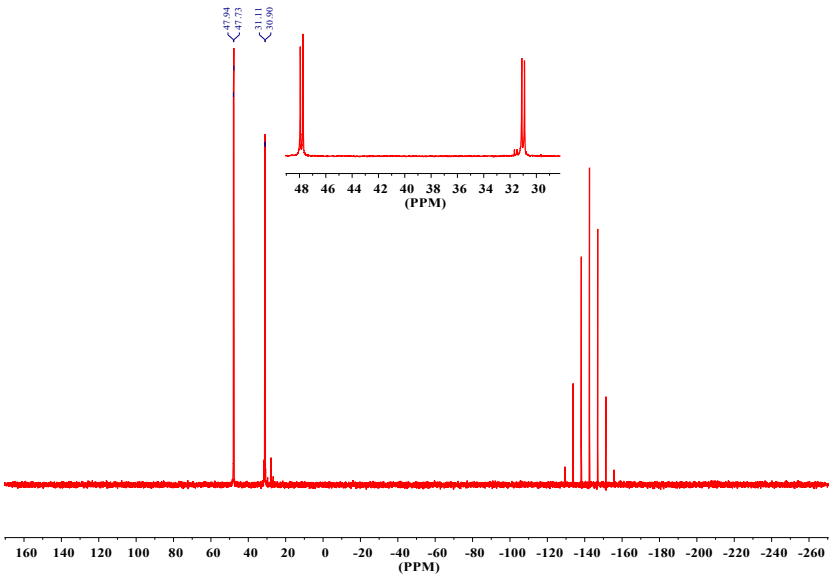

Figure S15. $^{31}P\{^{1}H\}$ NMR spectrum of complex (**2**) in CD_2Cl_2.

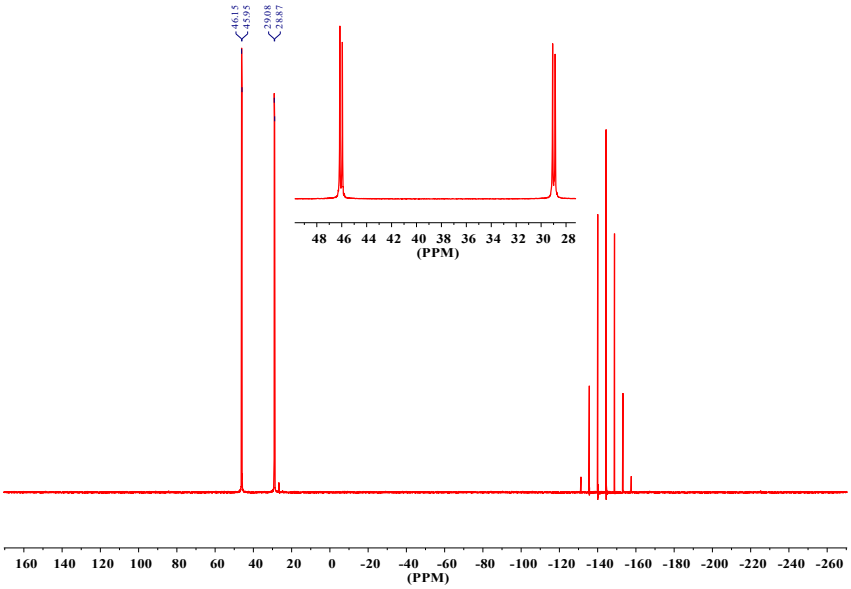

Figure S16. $^{31}P\{^{1}H\}$ NMR spectrum of complex (**3**) in CD_2Cl_2.

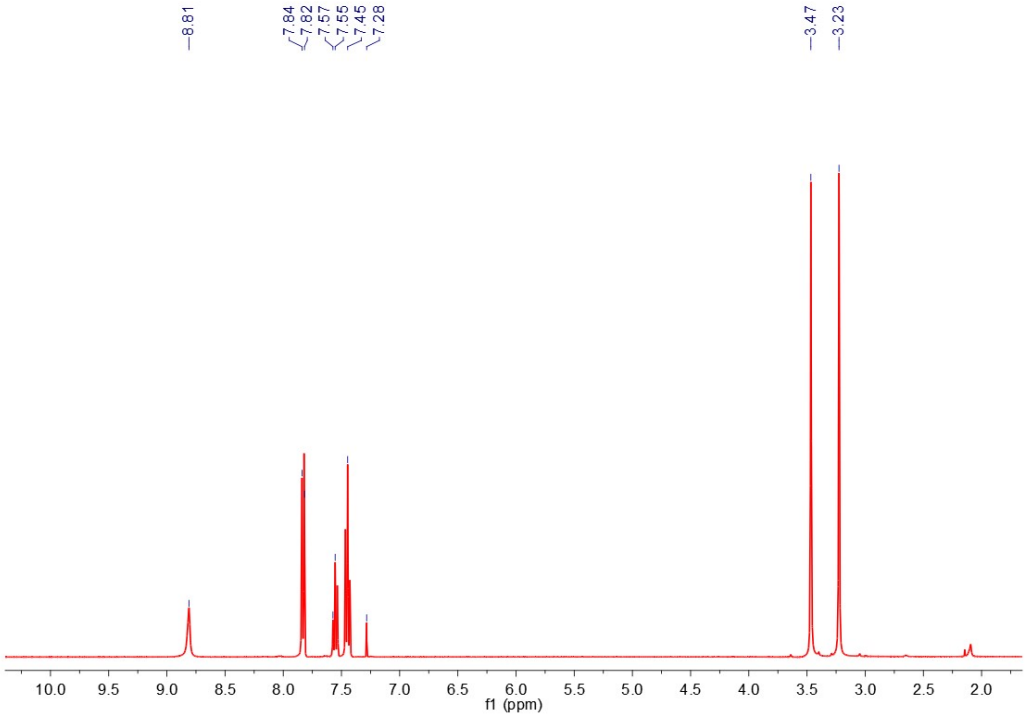

Figure S17. ^{1}H NMR spectrum of free *N,N*-dimethyl-*N'*-(benzoyl)thiourea in $CDCl_3$.

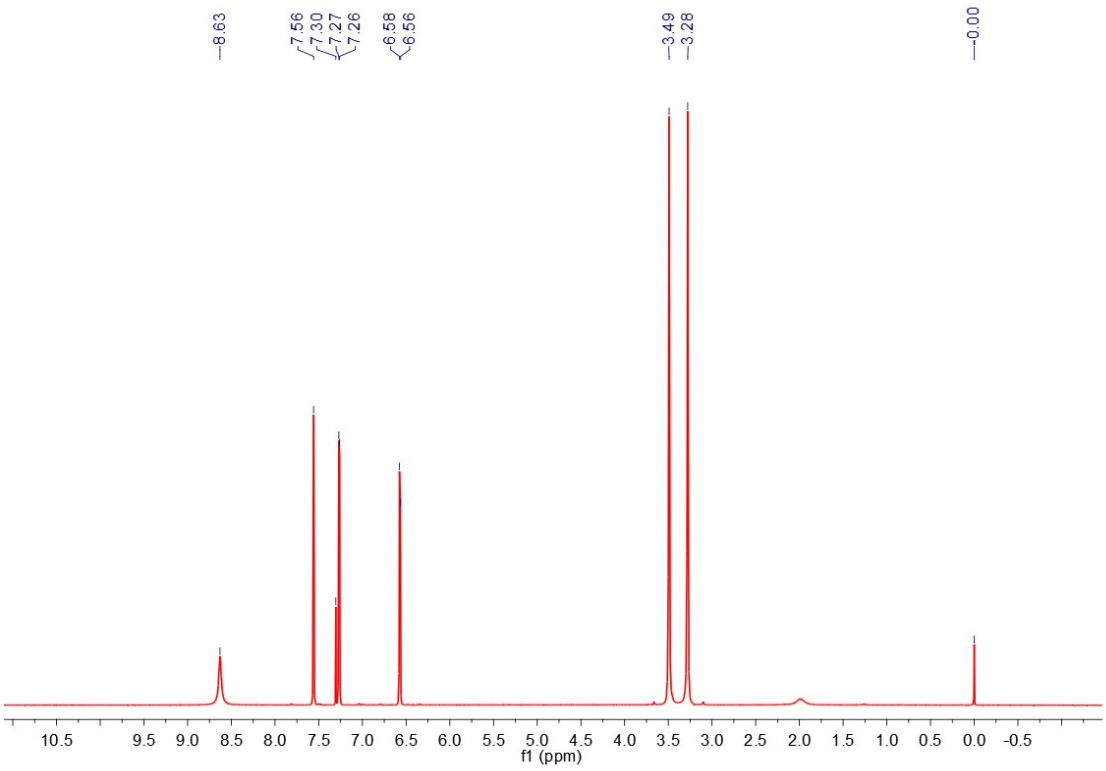

Figure S18. ^{1}H NMR spectrum of free *N,N*-dimethyl-*N'*-(furoyl)thiourea in $CDCl_3$.

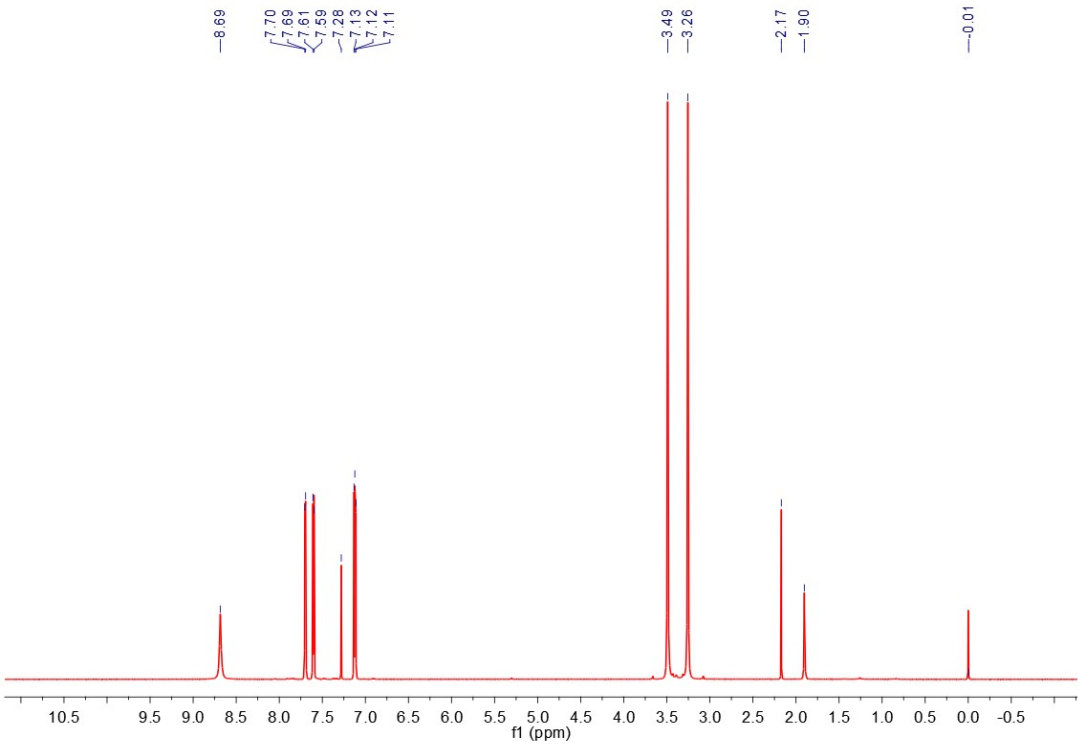

Figure S19. ^{1}H NMR spectrum of free *N,N*-dimethyl-*N'*-(thiophenyl)thiourea in $CDCl_3$.

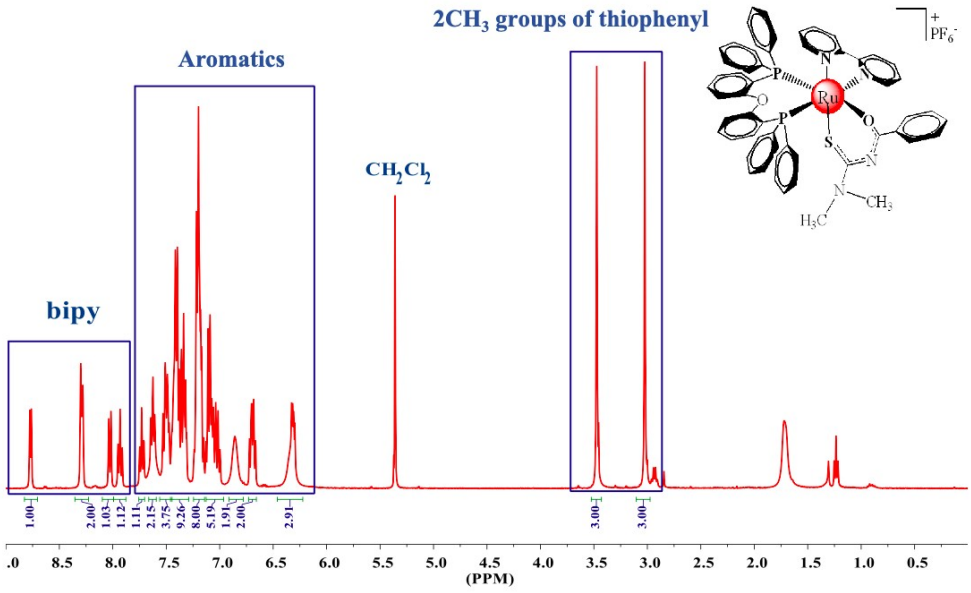

Figure S20. ^{1}H NMR spectrum of complex (**1**) in CD_2Cl_2.

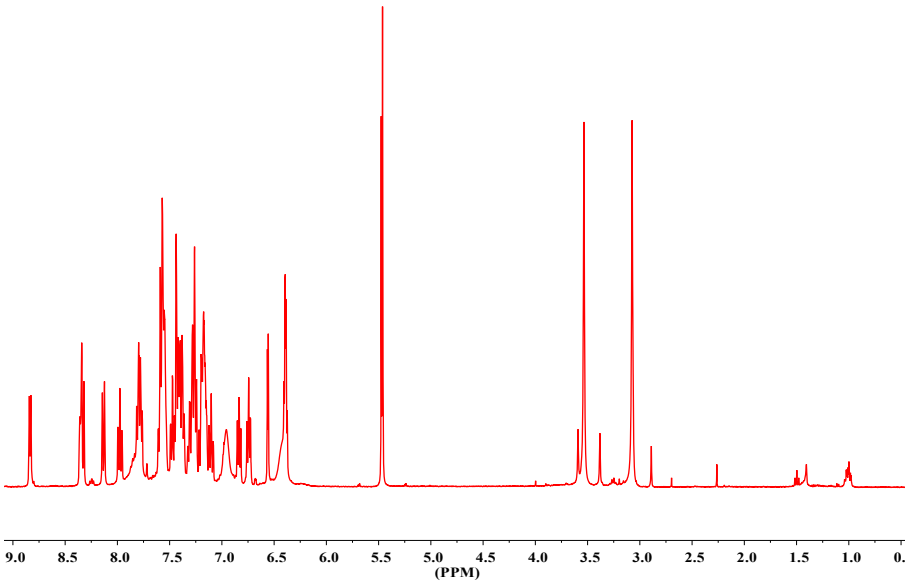

Figure S21. ^{1}H NMR spectrum of complex (**2**) in CD_2Cl_2.

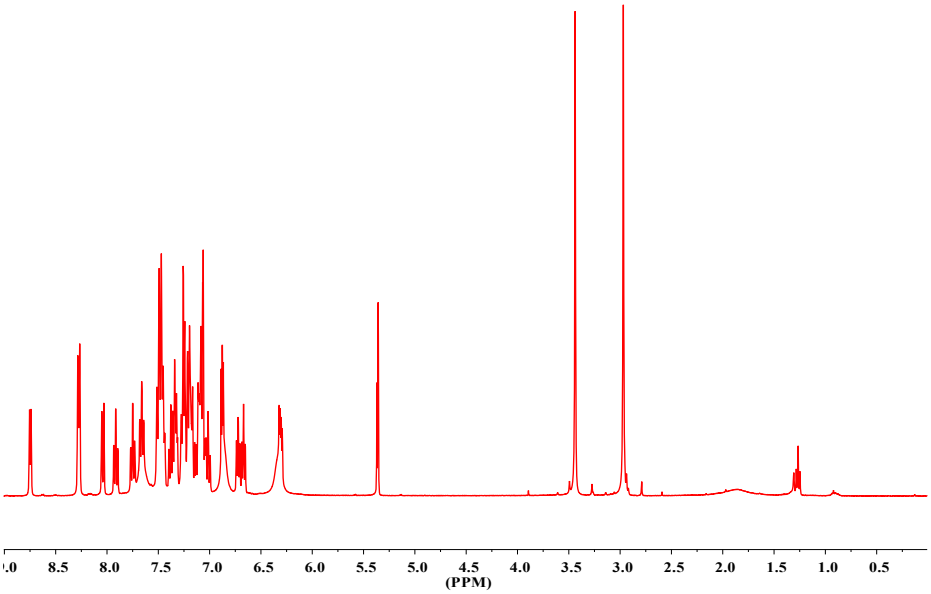

Figure S22. ^{1}H NMR spectrum of complex (**3**) in CD_2Cl_2.

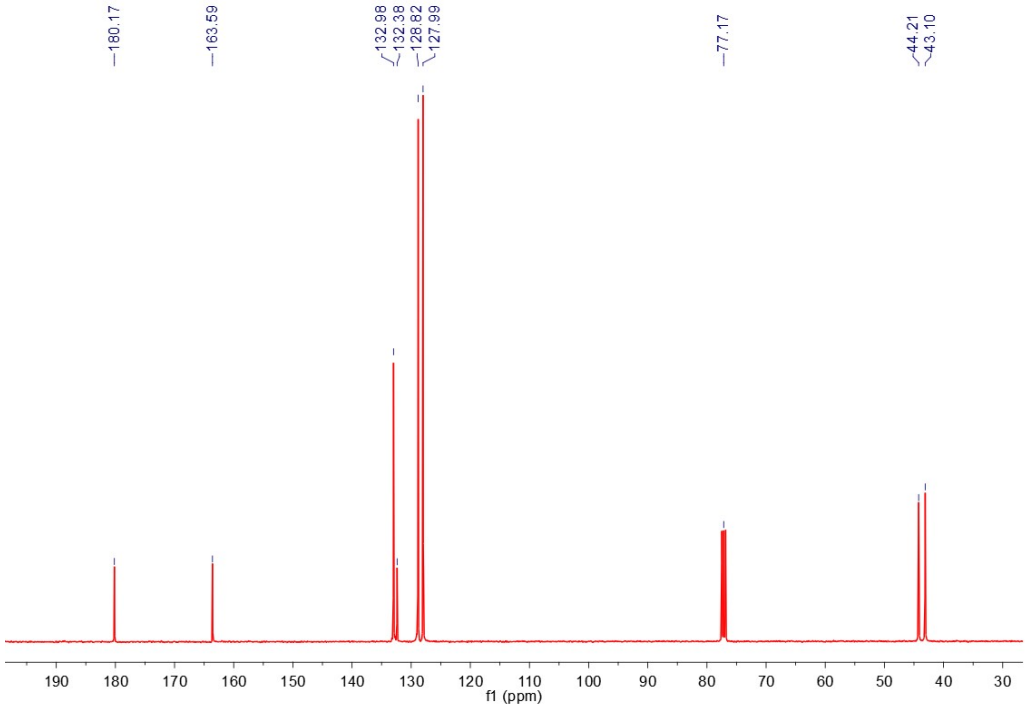

Figure S23. ^{13}C NMR spectrum of free *N,N*-dimethyl-*N'*-(benzoyl)thiourea in $CDCl_3$.

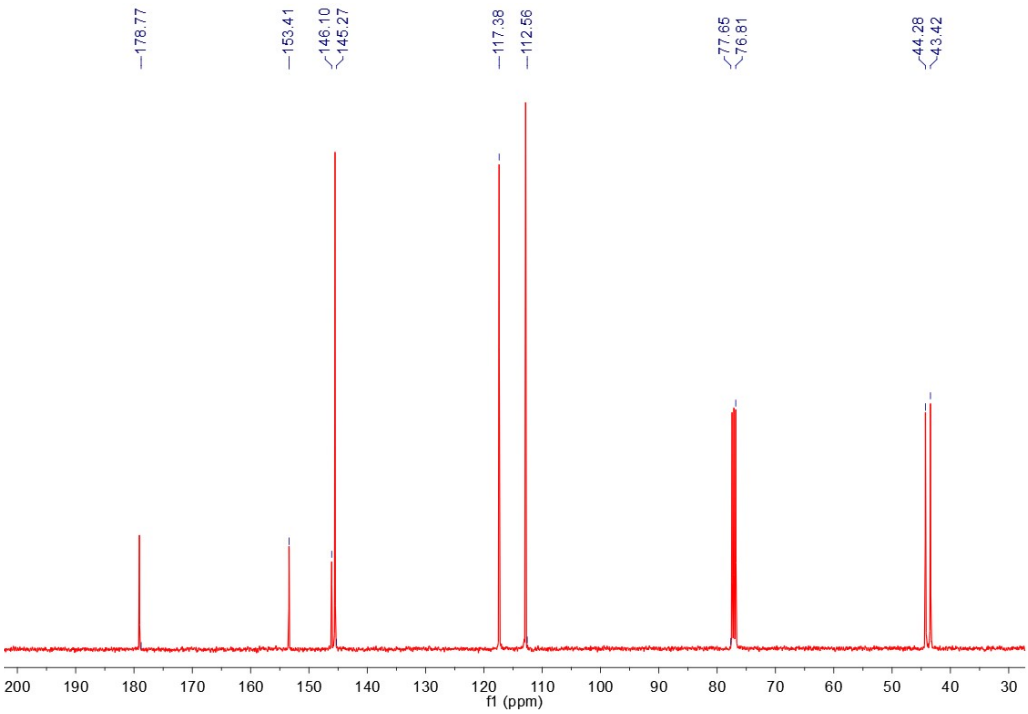

Figure S24. ^{13}C NMR spectrum of free *N,N*-dimethyl-*N'*-(furoyl)thiourea in $CDCl_3$.

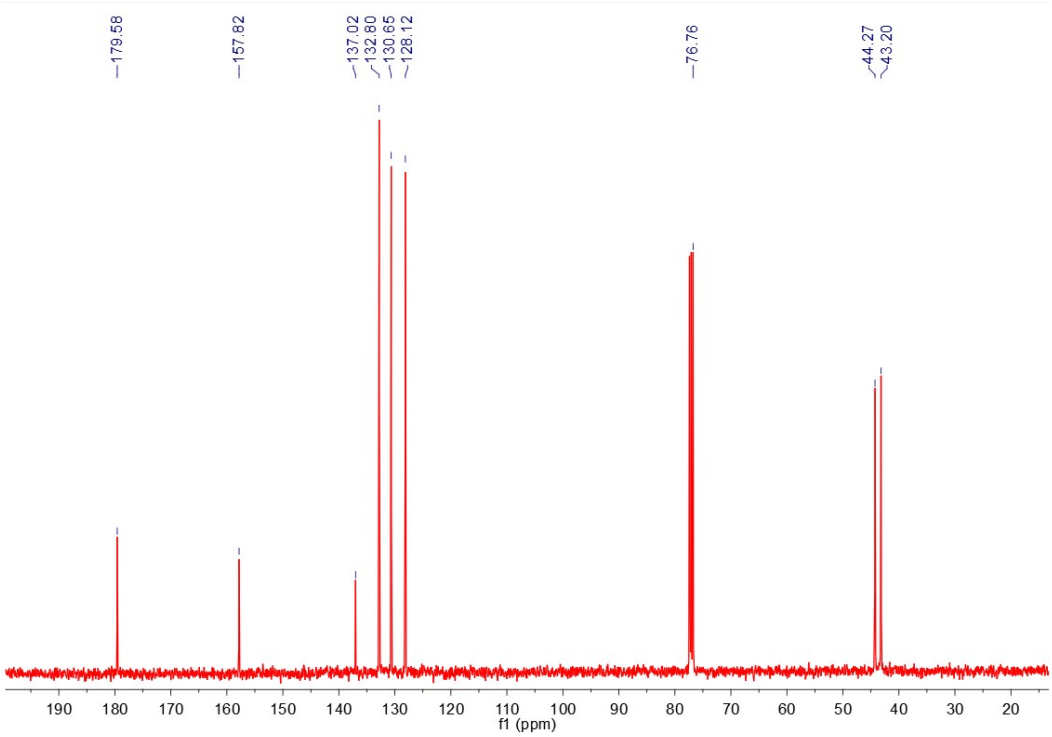

Figure S25. ^{13}C NMR spectrum of free *N,N*-dimethyl-*N'*-(thiophenyl)thiourea in $CDCl_3$.

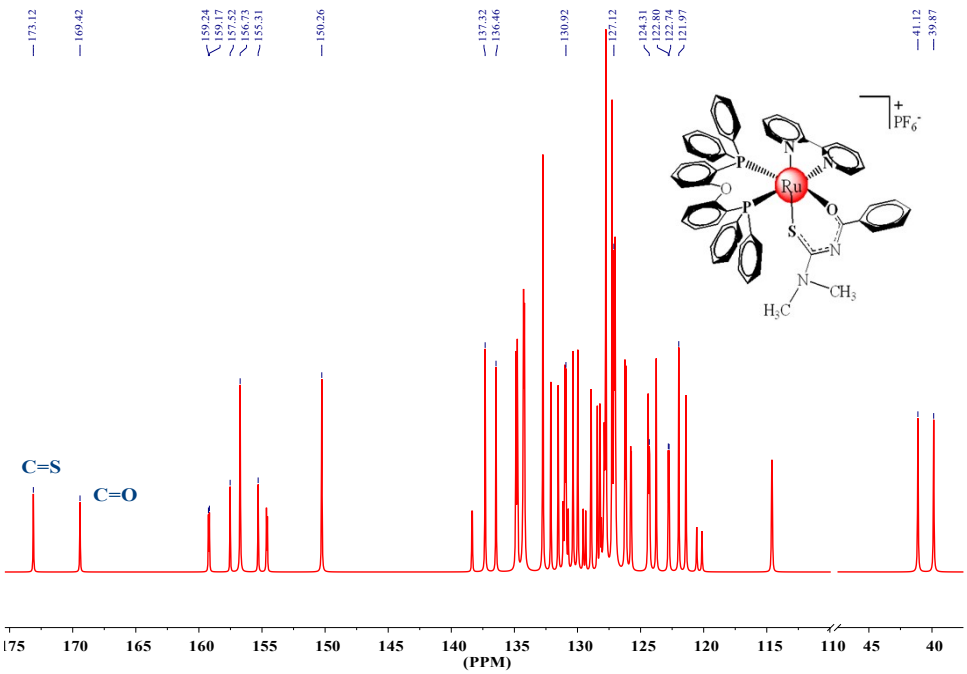

Figure S26. $^{13}C\{^1H\}$ NMR of complex (**1**) in CD_2Cl_2.

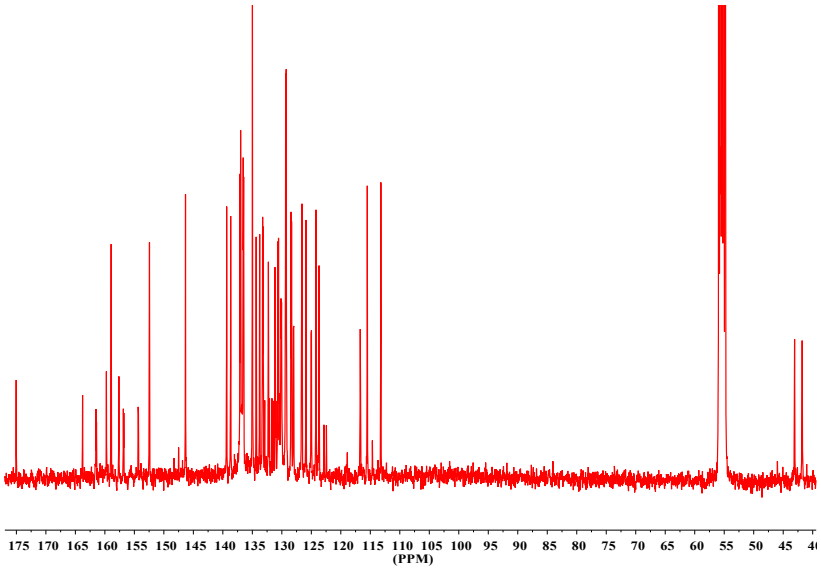

Figure S27. $^{13}C\{^{1}H\}$ NMR spectrum of complex (**2**) in CD_2Cl_2.

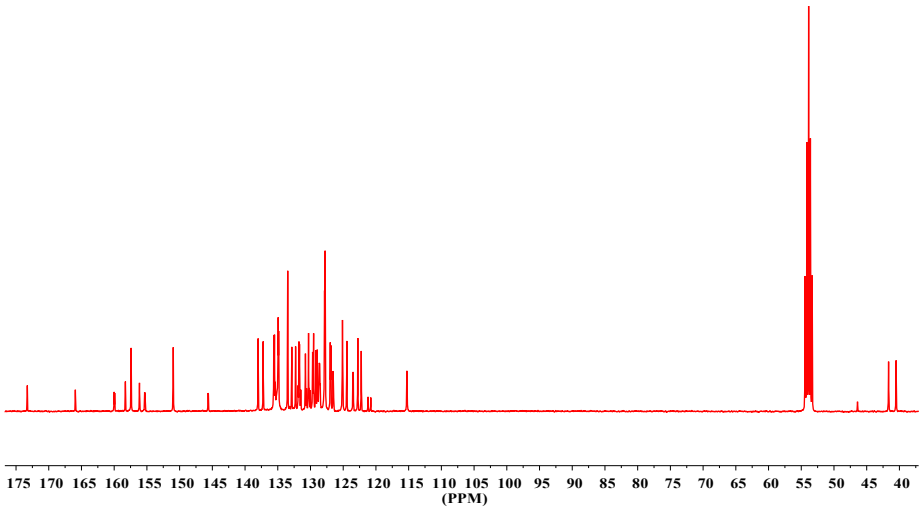

Figure S28. $^{13}C\{^{1}H\}$ NMR spectrum of complex (**3**) in CD_2Cl_2

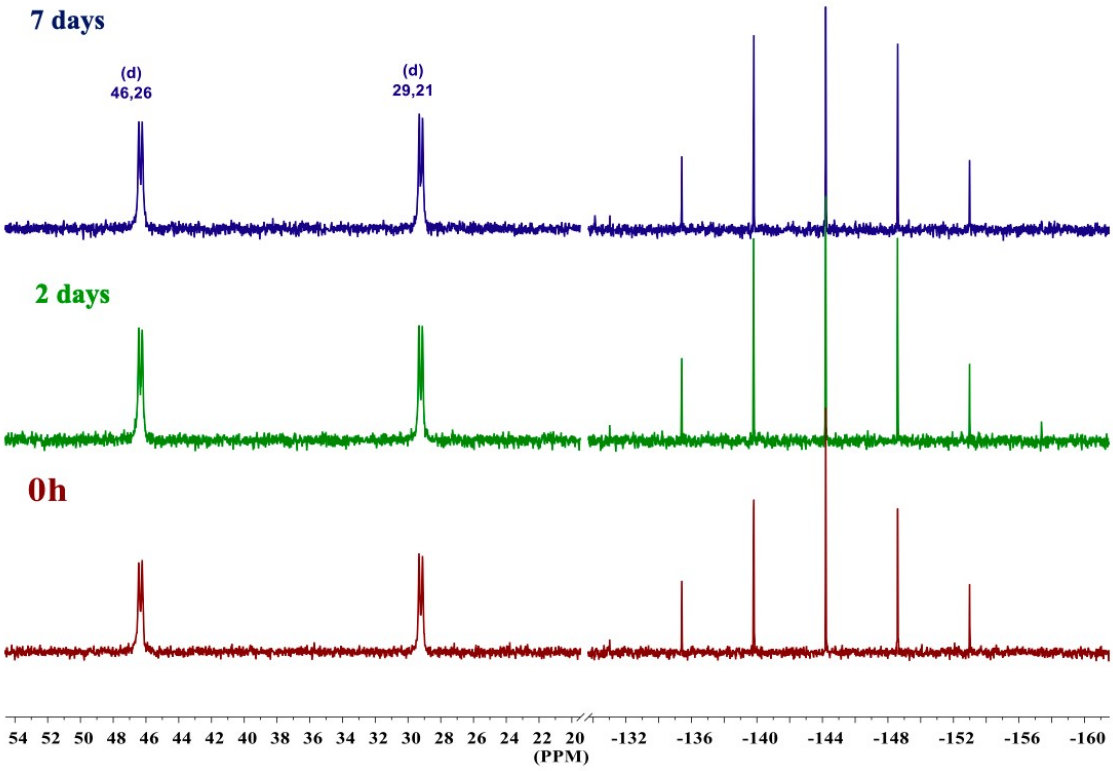

Figure S29. $^{31}P\{^{1}H\}$ NMR spectra of complex (**1**) in DMSO/DMEM 3:1 (v/v) at different times and room temperature.

Table S1. Crystal data and structure refinement for complex (**2**)

Empirical formula	$[RuC_{54}H_{45}N_4O_3P_2S]PF_6$
Formula weight	1137.98
Temperature	293(2) K
Wavelength	0.71073 Å
Crystal system	Orthorhombic
Space group	Pbcn
Unit cell dimensions	a = 19.3556(4) Å
	b = 22.3068(4) Å
	c = 23.0775(4) Å
Volume	9964.0(3) $Å^3$
Z	8
Density (calculated)	1.517 Mg/m^3
Absorption coefficient	0.525 mm^{-1}
F(000)	4640
Crystal size	0.493 x 0.485 x 0.269 mm^3
Theta range for data collection	2.747 to 25.999°.
Index ranges	$-23\leq h\leq 23$, $-27\leq k\leq 27$, $-28\leq l\leq 28$
Reflections collected	194061
Independent reflections	9788 [R(int) = 0.0564]
Completeness to theta = 25.242°	99.9 %
Refinement method	Full-matrix least-squares on F^2
Data / restraints / parameters	9788 / 0 / 690
Goodness-of-fit on F^2	1.288
Final R indices [I>2sigma(I)]	R1 = 0.0500, wR2 = 0.0961
R indices (all data)	R1 = 0.0796, wR2 = 0.1252
Largest diff. peak and hole	0.623 and -0.795 $e.Å^{-3}$

Table S2. Selected bond lengths [Å] for complex (**2**)

Ru(1)-O(1)	2.114(3)	O(2)-C(3)	1.350(7)
Ru(1)-N(3)	2.116(4)	O(2)-C(6)	1.373(7)
Ru(1)-N(4)	2.138(3)	O(3)-C(212)	1.386(6)
Ru(1)-P(1)	2.2958(11)	O(3)-C(112)	1.387(5)
Ru(1)-P(2)	2.3476(11)	N(2)-C(2)	1.347(6)
Ru(1)-S(1)	2.3506(11)	N(2)-C(8)	1.448(7)
S(1)-C(2)	1.733(5)	N(2)-C(7)	1.457(7)
P(2)-C(211)	1.821(4)	N(1)-C(1)	1.310(6)
P(2)-C(221)	1.833(5)	N(1)-C(2)	1.320(6)
P(2)-C(231)	1.840(5)	N(4)-C(18)	1.325(5)
P(1)-C(131)	1.830(5)	N(4)-C(14)	1.341(6)
P(1)-C(111)	1.840(5)	N(3)-C(9)	1.321(6)
P(1)-C(121)	1.841(5)	N(3)-C(13)	1.371(6)
O(1)-C(1)	1.264(5)		